# Velocity measurements within high velocity air-water jets

# Mesures de vitesses dans des jets eau-air à grandes vitesses

HUBERT CHANSON
*Department of Civil Engineering,*
*The University of Queensland,*
*St. Lucia QLD 4072, Australia*

**SUMMARY**
High velocity turbulent jets are often used in hydraulic structures to dissipate energy and to induce or enhance air entrainment. Examples include ski jumps and bottom aeration devices. This article presents new air concentration and velocity measurements performed in the flow development region of high velocity water jets. The measurements were obtained using a two-tips conductivity probe. The data are compared with analytical air concentration profiles derived from the diffusion equation, and theoretical velocity profiles of turbulent shear layers. The results highlight that the lower jet interface defined as $C = 90\%$ coincides with the streamline of maximum velocity gradient.

*Key words:* water jets, plane turbulent shear layers, air entrainment, dam, spillway, aeration device, ski jump.

**RÉSUMÉ**
Pour des structures hydrauliques, on utilise couramment des jets à grandes vitesses pour dissiper une grande partie de l'énergie, ou pour favoriser l'entraînement d'air. Des exemples typiques sont les sauts de ski ou les aérateurs de fond. Dans cet article, l'auteur présente de nouvelles mesures de concentrations en air et de vitesses, dans la partie initale du jet, pour des vitesses initiales de 7.6 et 10.6 m/s. Ces mesures ont été obtenues avec ue sonde de mesure de résistivité bi-point. On compare les mesures avec des résultats théoriques dérivés de l'équation de diffusion des bulles d'air, et de l'équation de quantité de mouvement. Les résultats indiquent clairement que l'interface air-eau, définie pour 90% de concentration en air, coïncide avec la ligne de courant où le gradient de vitesse est maximum.

*Mots clés:* jet d'eau, écoulement turbulent plan, entraînement d'air, barrage, déversoir, évacuateur de crues, aérateur, saut de ski.

## 1 Introduction

### 1.1 *Presentation*

High velocity turbulent jets are often used in hydraulic structures to dissipate energy and to induce or enhance air entrainment. Typical examples include jet flows downstream of a ski jump at the toe of a spillway, and flows above a bottom aeration device along a spillway (Fig. 1). With such high velocity jets, aeration occurs on both the upper and lower air-water interfaces (Ervine and Falvey 1987, Chanson 1989a).

Although ski jumps and bottom aerators have been installed for some years, the mechanisms of air entrainment along the jet free surfaces, and the interactions between air entrainment and the flow characteristics are not clear.

Revision received December 31, 1993. Open for discussion till December 31, 1994.

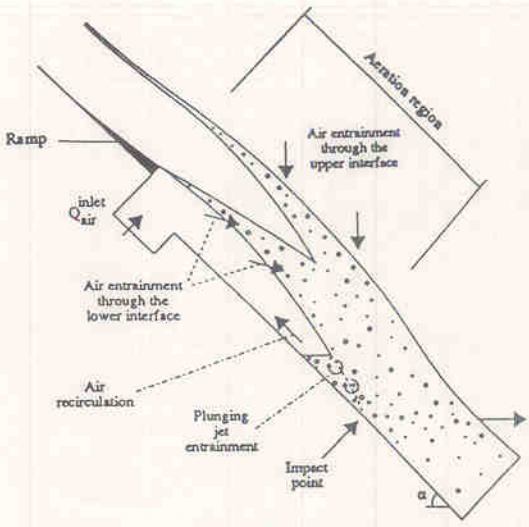


(a) Bottom aeration device.
Aérateur de fond.

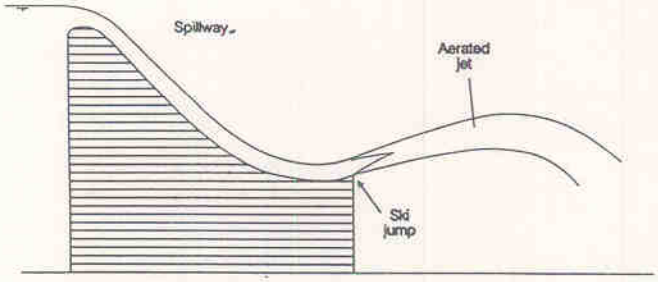


(b) Water jet downstream of a ski jump.
Jet en aval d'un saut de ski.

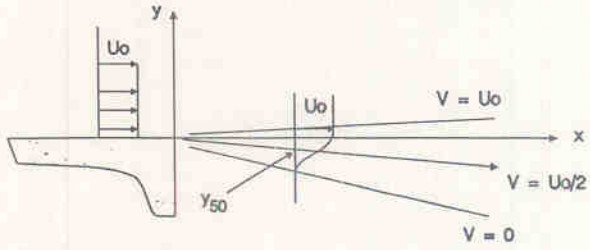


(c) Plane turbulent shear layer.
Jet plan turbulent.

Fig. 1. Examples of high velocity water jets.
Exemples de jet à grandes vitesses.

## 1.2 *Main flow regions*

With supercritical flows a small deflection in a chute structure (e.g. ramp, offset) tends to deflect the high velocity flow away from the chute surface (Fig. 1). In the cavity formed below the nappe (Fig. 1a), a local subpressure ($\Delta P$) is produced by which air is sucked into the flow. The flow regions that are described in the paper are the approach flow region, the transition region and the aeration region.

The approach flow conditions characterise the flow immediately upstream of a ski jump or an aerator ramp. The flow may be aerated. The transition region coincides with the length of the jump or the length of the ramp (Fig. 1a). A ramp or a ski jump increases the shear stress on the spillway bottom and the local pressure in the flow rises above hydrostatic. Both with and without a ramp there is a pressure change at the edge of the ramp from a quasi-hydrostatic pressure distribution to a zero (e.g. ski jump) or negative pressure gradient (e.g. bottom aerator). The pressure on the upper and lower free surfaces at the edge are respectively atmospheric and the cavity pressure ($P_{atm} - \Delta P$).

From the lip of the deflector to the impact of the jet (i.e. aeration flow region) the flow is a two-dimensional jet subject to a zero (or negative) pressure gradient, and for high Froude numbers large quantities of air are entrained through both the upper and lower free surfaces. If the jet is

long enough, a fully-aerated jet region starts developing downstream of the point where the central part of the jet becomes aerated (Fig. 1a). At the edge of the deflector the intense shear at the surface of velocity discontinuity induces a high level of turbulence. As the air beneath the jet is accelerated and some air is entrained, a portion of the water jet loses some momentum.

### 1.3 *Bibliographic review*

Several papers analysed the characteristics of circular turbulent water jets with applications for fire-fighting equipment (Thorn 1974, Hoyt and Tailor 1977), nozzles for Pelton turbines (Dodu 1957) and mixing devices (Van de Sande and Smith 1973). Most studies used high-speed photographs to describe the jet flow. Kawakami (1973) discussed the effect of flow aeration on water jet lengths downstream of a ski jump using prototype data. A recent paper (Ervine and Falvey 1987) discussed the effects of air entrainment on the jet spreading and jet breakup. Three studies (Shi et al. 1983, Low 1986, Chanson 1988) performed air concentration measurements to investigate the diffusion of air bubbles in two-dimensional jets above bottom aeration devices. The results were reported elsewhere (Chanson 1989a,1992). But none of these works obtained velocity distributions in the air-water flow regions.

The object of this paper is to present air concentration and velocity measurements performed simultaneously above an aerator on the Clyde dam spillway model (New Zealand). The data were obtained in the flow development region ($x/d_0 < 20$) of high velocity jets ($U_w = 7.6$ and 10.6 m/s). New instrumentation and data acquisition systems were used to perform these air concentration and velocity measurements. Later the results are compared with plane turbulent shear layers.

## 2 Experiments

### 2.1 *Description*

The author performed experiments on a 1:15 scale model of the Clyde dam spillway with a slope $\alpha = 52.33$ degrees and a channel width $W = 0.25$ m (Chanson 1988). Air concentration and velocity measurements were performed simultaneously along the 3.73 m long channel for two flow conditions (Table 1). The aerator configuration included an offset of 30 mm height, no ramp and a groove, and is similar to the geometry used by Tan (1984).

Table 1. Experimental flow conditions / Conditions d'expérimentations

| Run No. (1) | $q_w$ $m^2/s$ (2) | $d_0$* m (3) | $(U_w)_0$* m/s (4) | $Fr_0$ (5) | $Q_{air}^{inlet}/Q_w$ (6) | $P_N$ (7) | $x/d_0$ (8) |
|---|---|---|---|---|---|---|---|
| 1050 | 0.266 | 0.0352 | 7.6 | 12.9 | 0.541 | 0.006 | 0<br>4.35<br>11.1<br>18.24 |
| 1051 | 0.364 | 0.0345 | 10.6 | 18.1 | 0.495 | 0.026 | 0<br>3.68<br>11.6 |

Note: $\alpha = 52.33$ degrees - $t_s = 0.03$ m - $W = 0.25$ m - No ramp
* measured at the edge of the offset
$Fr_0 = (U_w)_0/\sqrt{g*d_0}$
$Q_{air}^{inlet}$: air discharge supplied to the cavity below the jet
$P_N = \Delta P/(\varrho_w * g * d_0)$
$x$: location of the measurement cross-sections

### 2.2 *Approach flow conditions*

The velocity distributions and velocity fluctuation distributions at the end of the deflector were measured in non-aerated flows using the Pitot tube described in the next paragraph. The results are reported on Fig. 6 and indicate that the turbulence intensity is around 1% outside the boundary layer. Near the spillway surface the effect of the boundary layer increases the turbulence intensity which becomes roughly 2–3%.

It must be emphasised that the distance between the flume intake and the edge of the deflector (0.303 m) is too short to obtain a fully developed bounary layer. Further at low discharges (i.e. Run No. 1050) the centreline velocity ($V \approx 8.7$ m/s) departs from the average flow velocity $(U_w)_0 = 7.6$ m/s (table 1). It is suggested that the difference results from the three-dimensional effects of the lateral boundary layers on the side walls (Chanson 1988).

### 2.3 *Instrumentation*

The pressure differences needed in the determination of the cavity subpressure were made with a very sensitive micro-manometer type 612a which enables reading down to 0.01 mm liquid column (distiled water). Clear water velocity and turbulence intensity measurements were performed with a Pitot tube and a pressure transducer scanned with a rate of 400 Hz in accordance with previous experiments (Ervine et al. 1980). The Pitot tube had an external diameter $\varnothing = 3.3$ mm and the pressure head at the tip was measured through a 1.1 mm hole. The distance between the tip of the probe and the lateral pressure points ($\varnothing = 0.5$ mm) was 20 mm. Before each measurement, air present in the Pitot tube was purged by injecting clear water at a pressure higher than the total head.

The air concentration and velocity measurements were obtained using a two-tip conductivity probe (described in the next paragraph) excited by an air bubble detector (AS25240) connected to a high speed data acquisition. The electronic circuit (i.e. air bubble detector) was calibrated with a square wave generator. Most of the measurements were recorded with a scan rate of 10 kHz per channel over 1.2 seconds of acquisition time.

### 2.4 *Two-tips conductivity probe*

#### Conductivity probe and air concentration

The principle of measurement is based on the difference in electrical resistivity between air and water. The resistance of the water is one thousand times lower than the resistance of air bubbles. Herringe (1973) showed that a needle resistivity probe gives accurate information regarding the local void fluctuations with a response signal indicating the presence of either air or water. When the probe tip is in contact with water, current will flow between the tip and the supporting metal; when it is in contact with air no current will flow. The local air concentration is the proportion of the total time that the probe tip is in the air.

The velocity probe included two identical tips. Each tip was a sharpened rod (platinum wire $\varnothing = 0.2$ mm) which is insulated except for its tip and set into a metal supporting tube (stainless steel needle $\varnothing = 0.8$ mm) acting as the second electrode. The insulation between the electrodes was made in standard Araldite resin.

For the probe described above, the author (Chanson 1988) estimated the errors on the local air concentration as:

$$\frac{\Delta C}{C} = 2\% \quad \text{for} \quad 5 < C < 95\% \tag{1a}$$

$$\Delta C = 2\% \quad \text{for} \quad C > 95\% \tag{1b}$$

$$\Delta C = 5\% \quad \text{for} \quad C < 5\% \tag{1c}$$

where $C$ is the air concentration[1].

## Principle of velocity measurement

In clear water velocities may be measured from pressure difference across a Pitot tube. In an air-water mixture air bubbles can be trapped in the tubes and lead inaccurate readings. Serizawa et al., (1975) and Cain (1978) used double-tip conductivity probes to measure air-water velocities based on a cross-correlation technique between the two tips aligned in the direction of the flow (Fig. 2). The cross-correlation function between the two tip signals is maximum for the average time taken for a bubble or a droplet to travel from the first tip to the second tip. The velocity can be calculated from the time delay between the signals and the tip separation distance.
In practice the signal from the second tip is disturbed by the first one. The cross-correlation method provides the probable time delay as the one for the maximum cross-correlation coefficient.

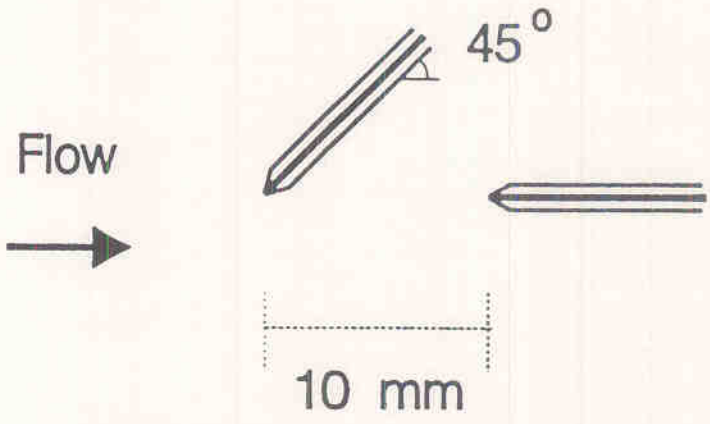


Fig. 2. Details of the velocity probe.
Détail de la sonde de mesure de vitesses.

## Design of the probe

The tip dimensions and spacing must be related to the characteristic dimensions of the air-water interfaces to be measured. On the Clyde dam spillway model high speed photographs indicate that the size of most bubbles is in the range 0.3 to 4.0 mm for $C = 50\%$ (Chanson 1988). The dimensions of the probe tips and the tip spacing were selected to detect these bubbles. The probe was designed with a small inner wire made of platinum ($\varnothing = 0.2$ mm) and the tips were spaced 10 mm apart (Fig. 2). The probe characteristics are compared with other two-tips conductivity probes in Table 2. The accuracy of the probe is estimated as:

$$\frac{\Delta V}{V} = 10\% \quad \text{for} \quad C > 5\% \tag{2}$$

With a similar probe design Cain (1978) indicated velocity error of 3% on prototype spillway with large air bubbles. On spillway model the velocity error is larger because of the limitation of the instrumentation and the smaller bubble sizes.

[1] The air concentration (i.e. void ratio) is defined as the volume of air per unit volume of air and water.

Table 2. Velocity measurements using of two-tip conductivity probes
Mesures de vitesses avec des sondes de résistivité bipoints

| Exp. (1) | $q_s$ $m^2/s$ (2) | $U_w$ m/s (3) | Distance between tips (4) | Scanning time (5) | Scanning rate (6) | $d_{b_{min}}$ (7) | Remarks (8) |
|---|---|---|---|---|---|---|---|
| (I) | | 0.5 to 2 | 5 mm | 1 to 3 mm | | 0.2 mm | Bubbly pipe flows |
| (II) | 2.2 and 3.2 | 15.6 to 18.5 | 101.6 mm | 15 and 60 s | 500 Hz to 4 kHz | 2 mm | Prototype spillway |
| (III) | 0.26 to 0.4 | 7 to 17 | 10 mm | 1.2 s | 10 and 20 kHz | 0.3 mm | Spillway model |

Note: $U_w$: average flow velocity
Scanning rate: scanning rate per channel
$d_{b_{min}}$: minimum air bubble size that can be detected
(I) Serizawa et al. (1975); (II) Cain (1978); (III) Chanson (1988)

## Test of the velocity probe

The two-tips conductivity probe provided both air concentration and velocity measurements. Air concentration data can be obtained using the signal of the first tip of the probe. The first tip was yawed with respect to the streamlines with an angle of 45 degrees (Fig. 2). Preliminary tests were performed to compare the output signals of the first tip and of a single-tip conductivity probe (with identical tip dimensions) placed parallel to the streamlines. The single-tip probe and the double-tips probe were mounted on a trolley in such way that each probe was located at the same distance from the bottom. The velocity probe was installed on the centreline and the single-tip probe was 55 mm beside. The results indicated no effect of the probe yaw on the air concentration measurements as observed in high velocity turbulent flows by Nassos and Bankoff (1967) and Sene (1984).

A second series of test was carried out by mounting the velocity probe and the Pitot tube on the same trolley. The velocity probe was installed on the centreline and the Pitot tube was 55 mm beside. Air concentration data were deduced from the voltage across the first tip of the velocity probe. High speed photographs enabled an estimate of the bubble sizes. Fig. 3 presents the velocity distributions at the end of the flume (3.6 m from the end of the deflector). The data were obtained with mean air concentrations in the range 0.18 up to 0.41. The results are presented as $y/Y_{90}$ versus $V/V_{90}$ for the Pitot tube and velocity probe data, and compared with the 1/6th power law profile observed on Aviemore spillway (Cain and Wood 1981, Chanson 1989b), where $y$ is the distance measured perpendicular to the bottom, $Y_{90}$ is the depth where the local air concentration is 0.90, $V$ is the local velocity and $V_{90}$ is the velocity at $Y_{90}$ which was calculated from the continuity equation (Chanson 1989b).

Close to the bottom (i.e. for low local air concentrations) Fig. 3 shows a good agreement between the two probes. When the distance from the bottom increase, the bubble concentration increases and the Pitot tube data are unreliable as air bubbles may be trapped in the holes of the tube (i.e. for $C > 0.30$). Away from the channel surface (i.e. $y/Y_{90} > 0.8$) the air concentration ratios are large ($C > 80\%$) and the oscilloscope allows visual correlation between the two tips of the velocity probes. This indication confirms the velocity results from the cross-correlation computations. It must be noted that, at low air concentrations ($C < 40\%$), a wake behind the first probe filled with air is observed and this wake includes the second tip. Sene (1984) observed also the presence of a wake behind a probe placed perpendicular to the mean flow. In such cases, the correlation

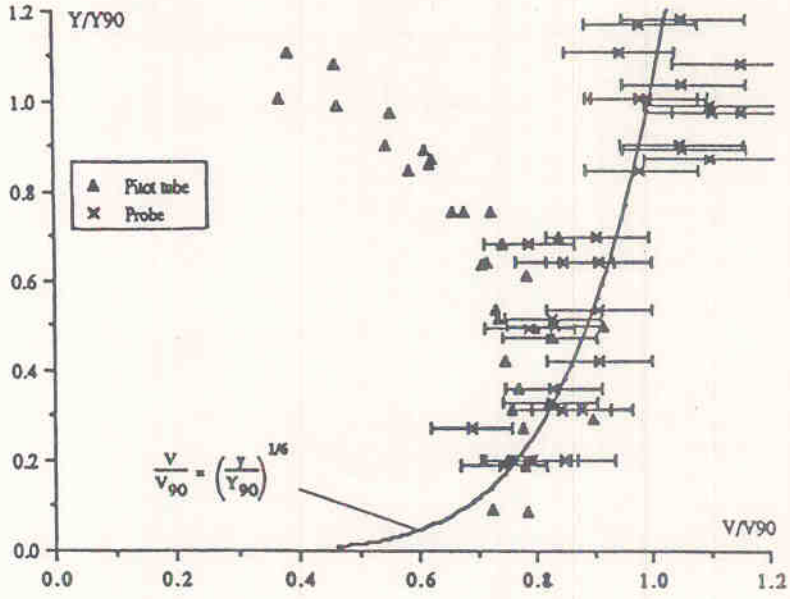


Fig. 3. Comparison of velocity data.
Comparaison des mesures de vitesses.

between the signals becomes negative (Fig. 4) but the velocity data obtained by cross-correlation agrees with the Pitot tube readings. It is thought that, when an air bubble hits the first tip, the wake behind the tip is disturbed or destroyed, and the air bubble could propagate to the second tip at a velocity equal to the local flow velocity. When the air concentration increases, the passage from a negative to positive correlation gives a region where it is not possible to get a reasonable result.

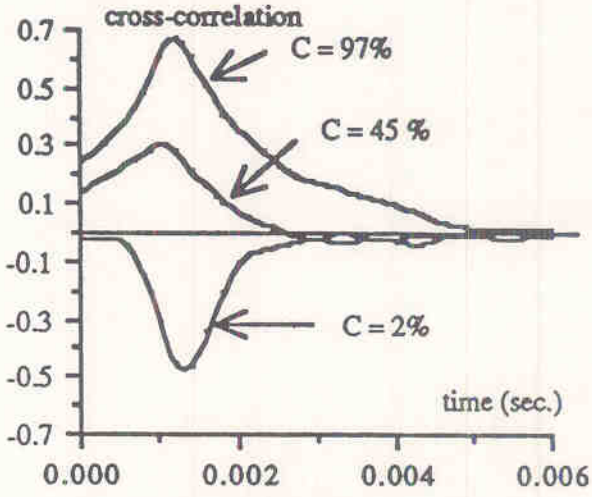


Fig. 4. Cross-correlograms – Data.
Cross-corrélogrammes.

From the air concentration and velocity distributions it is possible to verify the continuity equation with the data from the Pitot tube and the velocity probe. The results are presented in Fig. 5 where the water discharge $q_w$ per unit width defined as:

$$q_w = \int_0^{Y_{90}} (1 - C) * V * dy \tag{3}$$

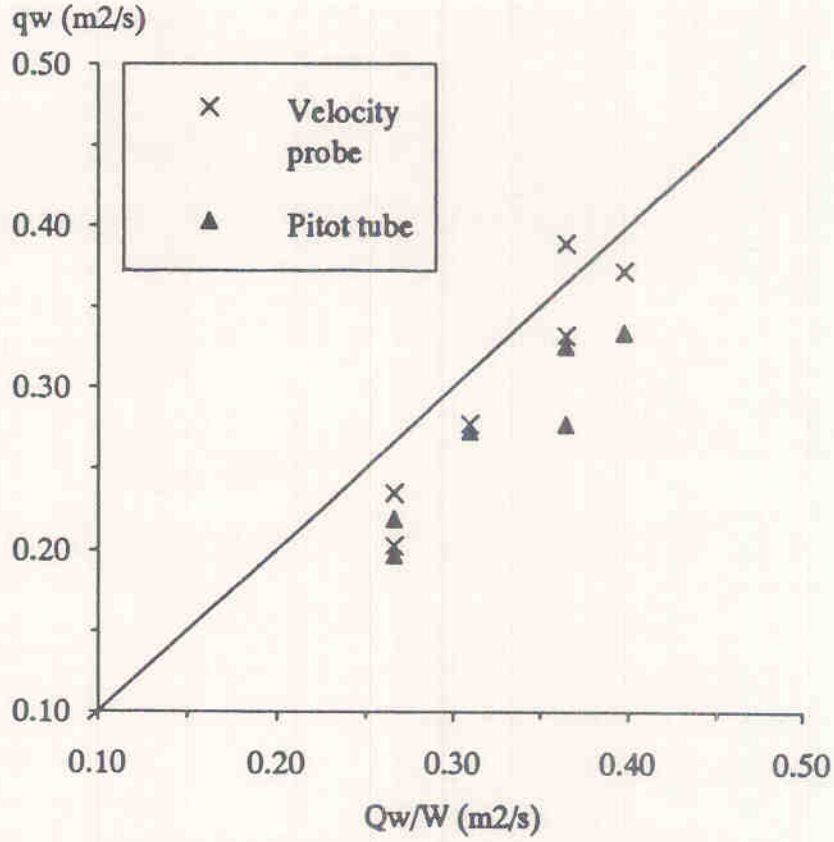


Fig. 5. Verification of the continuity equation.
Vérification de la conservation de la masse.

is computed with the air concentration and velocity measurements obtained with both the velocity probe and the Pitot tube. The upper limit $Y_{90}$ is estimated from the air concentration profiles with an error less than 0.2 mm. Fig. 5 presents equation [3] (i.e. $q_w$) as a function of the water discharge $Q_w/W$ for experimental data obtained by the author (Chanson 1988). It is estimated that the side effects are small and within the accuracy on the measurements. Fig. 5 shows that the estimate from the data obtained with the velocity probe is reasonable.
In summary this velocity probe enables simultaneous measurements of air concentration and velocity in high velocity air-water mixture.

### 2.5 *Discussion on air-water flow measurements*

#### Air-water interface

For low air concentrations (i.e. $C < 40\%$) photographic observations indicate that the air-water mixture is a bubbly flow characterised by air bubbles and air pockets surrounded by a continuous water phase. For large air concentrations (i.e. $C > 60$ to $70\%$) the mixture consists of water droplets flowing in an air flow. In between (i.e. $40\% < C < 60$ to $70\%$) the flow is an undefinable air-water mixture. The air concentration and velocity distributions exhibit continuous curves with respect to the distance normal to the spillway bottom, and the transition from an air-in-water flow to water-in-air flow is continuous and smooth.
Cain (1978) and Ackers and Priestley (1985) indicated that the velocities of air and water are equal (no slip) between 0 to 90% of air concentration. The air water mixture behaves as a homogeneous mixture for local air concentrations less than 0.90. The author suggested to use the iso-air con-

centration line $C = 90\%$ as the air-water interface of the mixture, as the slip ratio $V_{air}/V_w$ no longer equals 1 for $C > 90\%$ (Chanson 1991).

Velocity measurements

For large air concentrations ($C > 60$ to 70%), an oscilloscope allows visual correlation between the two tips of the velocity probe and confirms the velocity results by cross-correlation computations. Further it shows that the maximum correlation between the two tip signals of the velocity probe is not only a function of the passage of the air-water interfaces, but is directly dependant of the transit time of the water droplets on the tips. The cross-correlation technique gives then the travel time of the water droplets between the two tips. For $40\% < C < 60$ to 70% the flow is an undefinable air-water mixture and the technique of measurements gives the average velocity of the mixture. For low air concentrations ($C < 40\%$) the mixture consists of bubbles surrounded by water. By the same kind of reasoning as for large air concentrations, the analysis of each tip signal suggests that the correlation technique provides the velocity of the air bubbles.

## 3 Results

### 3.1 *Presentation*

For two discharges (Table 1), velocity and air concentration measurements were performed in the aeration flow region. The data was taken at a distance $x = 0$, 0.153, 0.391 and 0.642 m during the run 1050, and at $x = 0$, 0.127 and 0.399 m for the run 1051. The profiles are presented on Figs. 7 and 8 where the origin of the vertical axis ($y = 0$) is taken at the edge of the deflector. On these figures, the distance from the lip of the aerator is indicated on the top axis. Each experiment was performed with low subpressures (Table 1).

The air concentration data were obtained using the first tip of the velocity probe. Aerated flow velocity measurements were obtained with the velocity probe described above. For non-aerated flows (i.e. for $C < 5\%$), the velocities and turbulent intensities were measured with the Pitot tube.

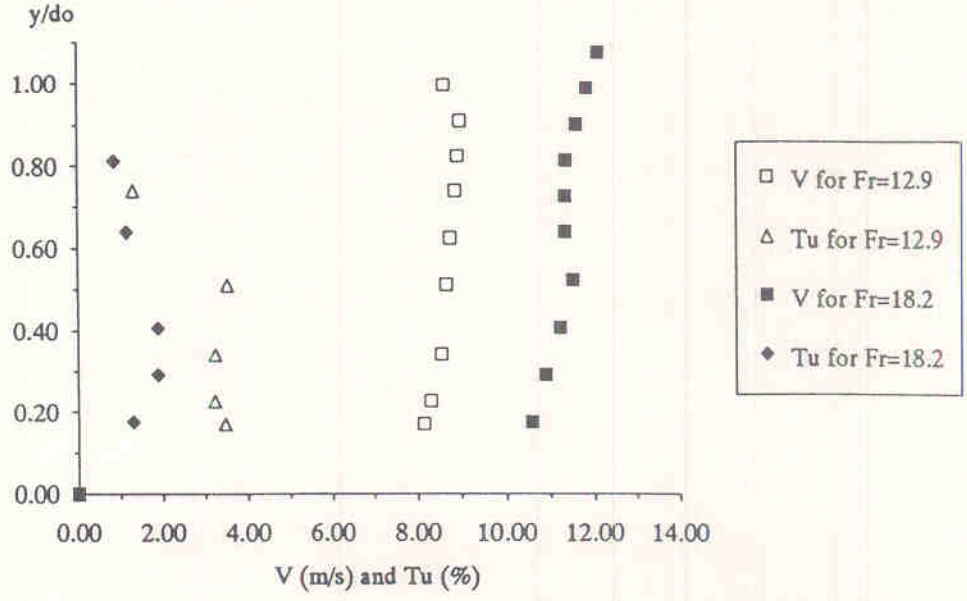


Fig. 6. Velocity and turbulence intensity at the end of the deflector - Ref. 1050 and 1051.
Vitesses et intensités turbulentes à la fin de la rampe - Réf. 1050 et 1051.

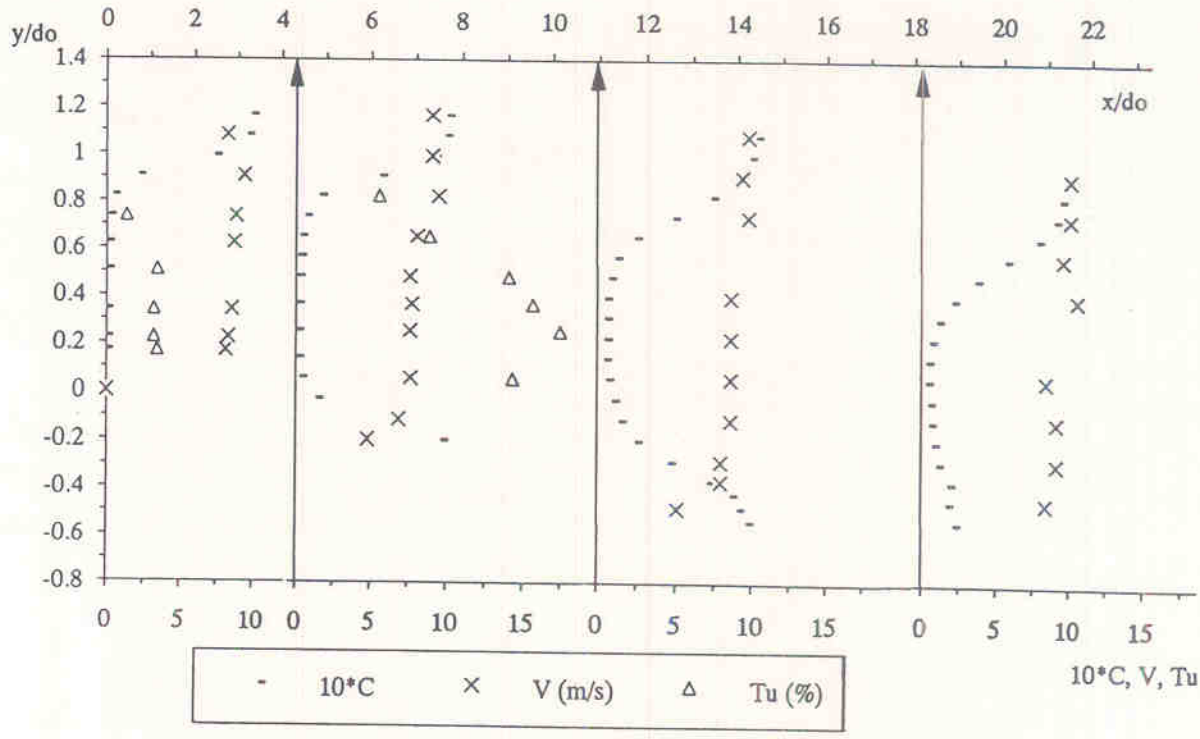


Fig. 7. Velocity measurements - Chanson (1988) - Ref. 1050.
Profils de vitesses - Chanson (1988) - Réf. 1050.

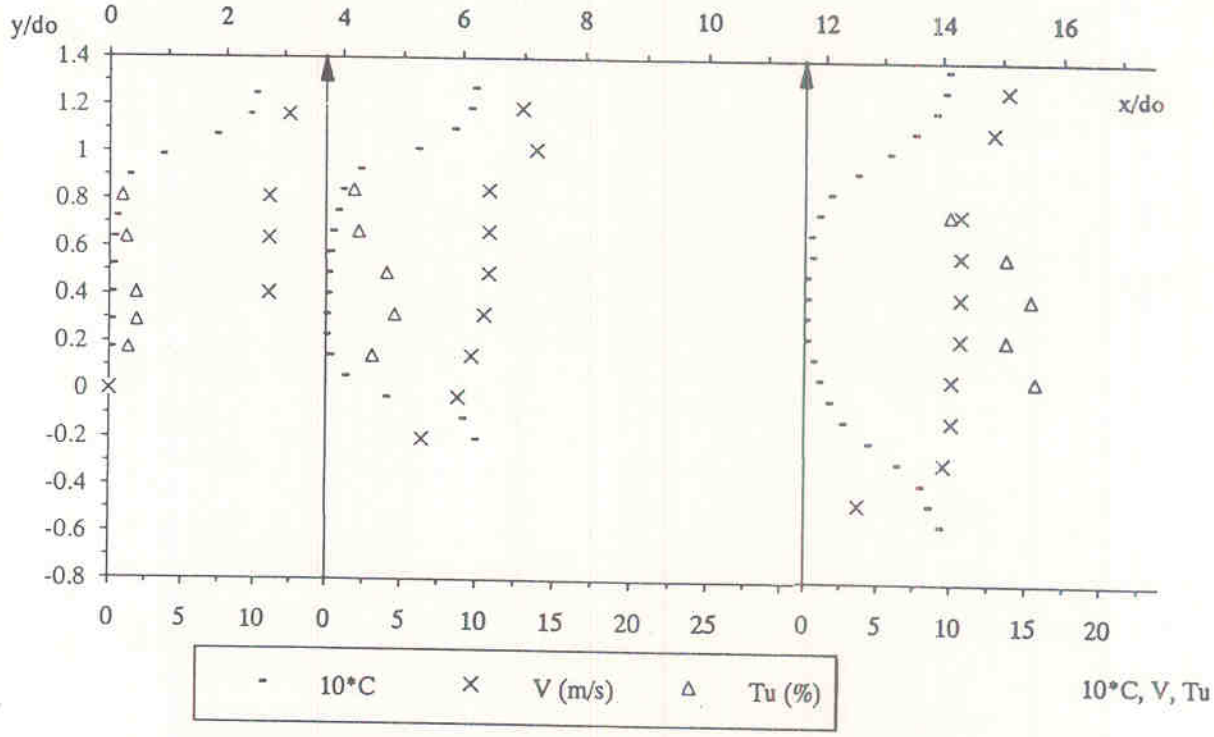


Fig. 8. Velocity measurements - Chanson (1988) - Ref. 1051.
Profils de vitesses - Chanson (1988) - Réf. 1051.

### 3.2 *Turbulence intensity*

At the end of the deflector a solid inner jet core of clear water (i.e. $C = 0\%$) is observed and it is reduced along the channel while the flow is aerated through the interfaces (Figs. 1, 7, 8). Figs. 7 and 8 show also the distributions of the root mean square of the value of axial component of the turbulent velocity $u'$ in the clear water core, measured with the Pitot tube.

The results indicate values of turbulence intensity $Tu = u'/V$ in the range 5 to 15% in the aeration region. These values must be compared with the initial distribution at the lip of the deflector in the range 1–3% (Fig. 6). Such an increase of turbulence intensity over a short distance (i.e. $\Delta u' \approx 1$ m/s for $\Delta x \approx 0.12$ m) may suggest a large increase of turbulent kinetic energy but also the possibility of jet oscillations affecting the measurements.

## 4 Discussion

### 4.1 *Air entrainment*

Chanson (1989a) analysed the diffusion of air bubbles on both the upper and lower free surfaces in the flow region with clear water core (Fig. 1), and showed that the air concentration distributions are estimated by:

$$C = \text{erf}\left(\frac{y}{\sqrt{2 * \frac{D^{upper}}{U_w} x * \left(1 + \frac{u_r}{U_w} * \cos\theta * \frac{y}{x}\right)}}\right) \quad \text{upper interface} \quad (4)$$

$$C = \text{erf}\left(\frac{y}{\sqrt{2 * \frac{D^{lower} + D^0}{U_w} * x}}\right) \quad \text{lower interface} \quad (5)$$

where $D^{upper}$ and $D^{lower}$ are the turbulent diffusivity at the upper and lower interfaces, $D^0$ is the effect of the longitudinal velocity gradient on the diffusivity at the lower interface, $u_r$ is the rise velocity of an air bubble within the jet (Chanson 1989a), $x$ is the distance along the spillway bottom from the end of the deflector, $y$ is the distance measured perpendicular to the spillway bottom (Fig. 1), $\theta$ is the angle between the streamline $x$ and the horizontal, and the function erf is defined as:

$$\text{erf}(u) = \frac{1}{\sqrt{\pi}} * \int_{-\infty}^{u} \exp(-t^2) * dt \quad (6)$$

When the flow leave the edge of the deflector, the water jet becomes subject to a zero or negative pressure gradient and the bubble rise velocity becomes a zero or fall velocity (Chanson 1989a). The author (Chanson 1991) detailed the calculations of this fall velocity as a function of the cavity subpressure. To a first approximation, the bubble size can be estimated as the critical bubble size in turbulent shear flows (see paragraph 4.3). The angle $\theta$ can be deduced at any position along the spillway from the jet trajectory equations (e.g. Schwartz and Nutt 1963, Tan 1984, Chanson 1988). At the upper and lower interfaces the diffusivities are estimated as:

$$D^{upper} = \frac{1}{2} * \frac{U_w * x}{1.2817} * (\tan \Psi^U)^2 \quad (7)$$

$$D^{lower} + D^0 = \frac{1}{2} * \frac{U_w * x}{1.2817} * (\tan \Psi^L)^2 \quad (8)$$

where $\Psi^U$ and $\Psi^L$ are the initial spread angle measured between $C = 10\%$ and $C = 90\%$, and $U_w$ is the flow velocity at the end of the deflector.

At the upper interface the upper spread angle is a function of the pressure gradient across the jet (Chanson 1991). For low subpressures the author obtained $\Psi^U = 0.75$ degrees. At the lower

interface the rapid change of bottom shear stress is dominant. For steep slopes the spread angle $\Psi^L$ is independent of the cavity subpressure, and may be estimated as:

$$\Psi^L = 0.698 * U_w^{0.630} \tag{19}$$

where $\Psi^L$ is in degrees and $U_w$ is in m/s. Equation [9] is an empirical correlation obtained from experiments detailed in appendix 1. For the two experiments (Figs. 7 and 8), equation [9] implies $\Psi^L = 2.5$ and 3.1 degrees.

On Fig. 9, the data are compared with the Gaussian distributions predicted from equations [4] and [5] at various positions along the jet. The bubble rise velocity was calculated as Chanson (1991) and $\theta$ was calculated from the jet calculations done using Chanson's (1988) method. The agreement is good. It can be noted that Ervine and Falvey (1987) observed also a Gaussian distribution for circular jets.

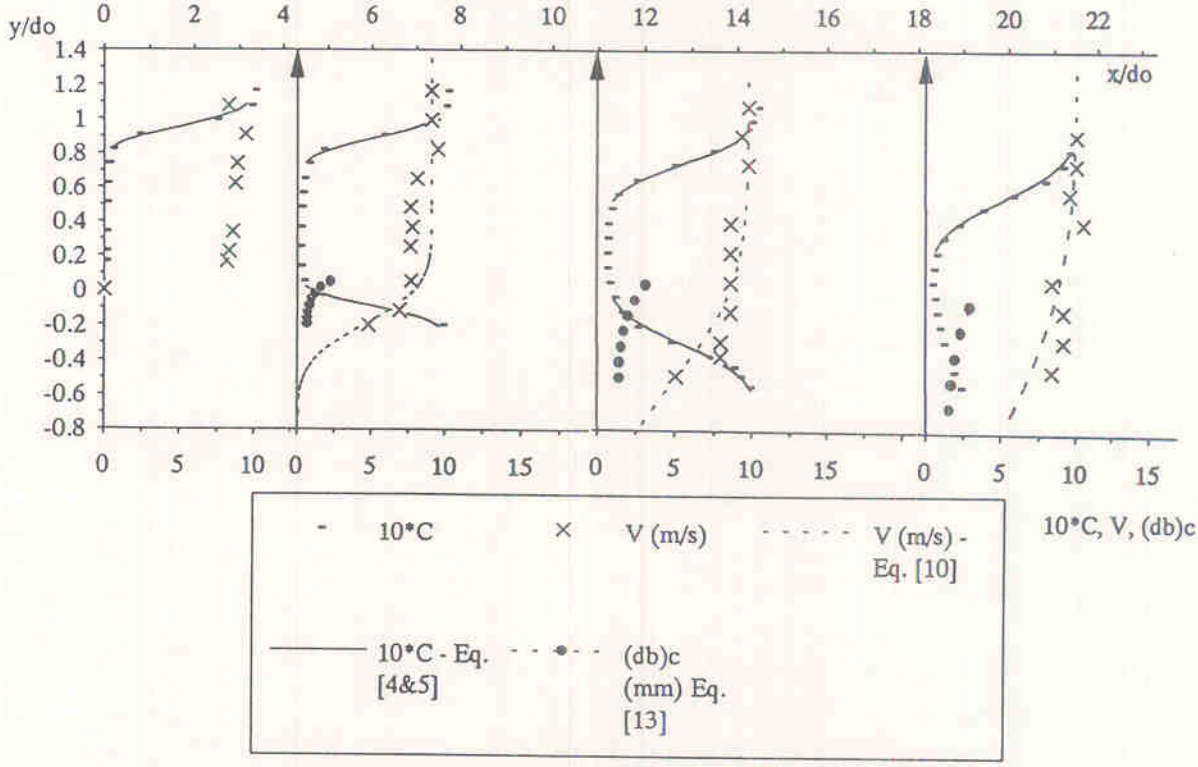


Fig. 9. Comparison between the data and equations [4], [5] and [10] - Ref. 1050.
Comparaison entre les mesures et les équations [4], [5] et [10]] - Réf. 1050.

### 4.2 *Velocity distribution*

For a plane horizontal jet of semi-infinite height or shear layer (Fig. 1C), Goertler (1942) solved the equations of motion assuming a constant eddy viscosity across the shear layer:

$$\nu_T = \frac{1}{4 * K^2} * x * U_0$$

where $\nu_T$ is the turbulent kinematic viscosity, $U_0$ the free stream velocity and $K$ a constant. Goertler (1942) obtained the solution in the first approximation (Rajaratnam 1976, Schlichting 1979):

$$V = U_0 * \text{erf}\left(\frac{K * (y - y_{50})}{x}\right)$$

where the function erf is defined in equation [6], $y$ is measured from the edge of the deflector and $y_{50}$ is the value of $y$ at the point where $V = U_0/2$ (Fig. 1C).

In the flow development region that is located upstream of the point where the shear layer reaches the upper free surface, it is reasonable to assume that the velocity at the upper interface of the jet $V_{90}^{upper}$ is the free stream velocity. Hence Goertler's (1942) solution becomes:

$$V = V_{90}^{upper} * \text{erf}\left(\frac{K * (y - y_{50})}{x}\right) \tag{10}$$

$$\nu_T = \frac{1}{4 * K^2} * x * V_{90}^{upper} \tag{11}$$

On Fig. 9, the velocity measurements are compared with equation [10] where $V_{90}^{upper}$ and $y_{50}$ were interpolated from the data at each cross-section, and the empirical constant $K$ was estimated as $K = 25.0$. Fig. 9 shows a reasonable agreement between the data and equations [4], [5] and [10]. It must be emphasised that equation [10] was obtained by neglecting:

1. the non uniform velocity distribution in the approach flow region;
2. the gravity and pressure effects;
3. the effects of air entrainment.

Further these calculations were done assuming a stagnant fluid (i.e. $V = 0$) in the cavity below the jet. For the particular case of a bottom aeration device, the air flow within the cavity is a function of the air discharge supplied to the cavity, the nappe entrainment, the plunging jet entrainment at the end of the cavity and the air recirculation (Chanson 1989a). At the present time there is little information available on these processes.

At the beginning of the jet the intense shear at the surface of velocity discontinuity induces high turbulence that is predominant at the lower free surface. As the air below the jet is accelerated, a portion of the water jet loses some momentum. This mechanism of momentum transfer is described by equations [10] and [11]. It must be noted that the estimated value of $K$ is larger than the values of 11.0 or 13.5 obtained respectively by Rajaratnam (1976) and Schlichting (1979).

On Fig. 10, the location of the turbulent shear layer is compared with the air concentration distribution. The position of the mid-velocity streamline $y_{50}$ is plotted as a function of the distance along the spillway, and compared with the iso-air concentration lines $C = 90\%$ and $C = 10\%$. The locations where $V = 0.9 * V_{90}^{upper}$ are shown also. It is worth noting that the point at which $V = V_{90}^{upper}/2$ (i.e. $y = y_{50}$) coincides almost with the lower air-water interface (i.e. $y = Y_{90}^{lower}$) for both sets of data.

The streamline $y = y_{50}$ is characterised by the maximum velocity gradient. Using Prandtl's mixing length hypothesis, and replacing the mixing length by a function of the turbulent viscosity and velocity gradient, the turbulent velocities parallel and normal to the flow direction are in the order of magnitude:

$$v' \sim u' \sim \sqrt{\nu_T * \frac{dV}{dy}}$$

Goertler (1942) assumed a constant eddy viscosity, and hence the turbulent velocities $u'$ and hence $v'$ are maximum on the streamline $y = y_{50}$. If the local air entrainment is assumed to be in the order of magnitude of $(C * v')$, the location at which the air entrainment is maximum coincides with the position where $C = 90\%$, and this result provides another reason for choosing $C = 90\%$ as the lower jet interface.

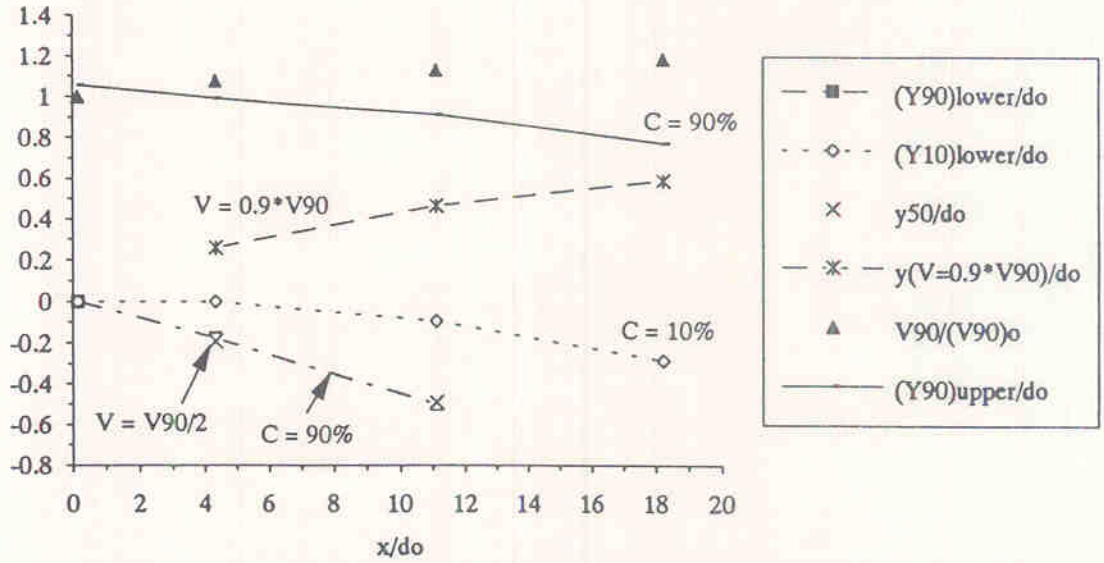


Fig. 10. Comparison between the air concentration layer and the shear layer - Ref. 1050.
Comparaison entre la distribution de concentration en air et le profil des vitesses - Réf. 1050.

As a consequence the velocity at the lower interface may be estimated as:

$$V_{90}^{\text{lower}} \sim 0.5 * V_{90}^{\text{upper}}$$

4.3 *Air bubbles in shear layers*

In the above section, the effects of air entrainment and the interactions between air bubbles and the turbulence have been neglected. Considering an air bubble in a turbulent shear flow, the maximum particle size is determined by the balance between the capillary force and the inertial force caused by the velocity change over distances of the order of the bubble diameter. Hinze (1955) showed that the splitting of air bubbles in water, or water droplets in air, occurs for:

$$\frac{\varrho_w * v^2 * d_b}{2 * \sigma} > (We)_c \tag{12}$$

where $d_b$ is the bubble size, $v^2$ the spatial average value of the square of the velocity differences over a distance equal to $d_b$, and $(We)_c$ a critical Weber number. Experiments showed that $(We)_c$ is a constant near unity: 0.59 (Hinze 1955), 1.26 (Sevik and Park 1973) and 1.02 (Killen 1982). A maximum particle size $(d_b)_c$ may be defined from the equation [12]. Assuming that the term $v^2$ is in order of magnitude of (Chanson 1992):

$$v^2 \sim \left(\frac{dV}{dy} * d_b\right)^2$$

and using equation [10], the maximum particle size in plane shear layers is in order of magnitude of:

$$(d_b)_c \sim \sqrt[3]{\frac{\sigma}{\varrho_w} * \frac{2 * \pi}{K^2} * \frac{x^2}{(V_{90}^{\text{upper}})^2 * \exp\left(-2 * \left(\frac{K * (y - y_{50})}{x}\right)^2\right)}} \tag{13}$$

Equation [13] is plotted in Fig. 9 and suggests that an upper limit to bubble size in the range 1 to

3 mm is the most likely to be present in the aerated bottom shear layer of the jet for this experiment. These values are similar to the author's photographic observations indicating bubble sizes of 0.3 to 4 mm (Chanson 1988).

## 5 Conclusion

New air concentration and velocity data obtained within aerated water jets are presented. The measurements were performed in the flow development region of two-dimensional high velocity jets.

Measurements were obtained using a two-tips conductivity probe. The probe enabled both air concentration and velocity measurements in bubbly air-water mixtures with local air concentrations in the range 0.05 to 0.95.

The air concentration data was compared with a diffusion model of air bubbles. A good agreement was obtained. The velocity data was compared with the velocity distributions obtained for plane turbulent shear layers as derived by Goertler (1942). A good agreement between the velocity data and Goertler's (1942) solution was obtained assuming a constant $K = 25$. The results show that the lower jet interface defined as $C = 90\%$ coincides with the streamline of maximum velocity gradient.

A simple estimation of the maximum bubble sizes was developed. The results suggest that small size bubbles are the most likely to be present within the aerated shear layer.


## 6 Acknowledgements

The author wishes to thank the Ministry of Works and Development (New Zealand) and the Department of Civil Engineering, University of Canterbury (New Zealand) for their support. He wishes also to acknowledge the contribution of Mr. A. Gardner, DSIR Electronics Section (New Zealand) for his help in designing and building the air bubble detector (AS25240).


## Notations

| | |
|---|---|
| $C$ | air concentration defined as the volume of air per unit volume |
| $D^{lower}$ | air concentration turbulent diffusivity at the lower air-water interface ($m^2/s$) |
| $D^0$ | air concentration diffusivity due to the longitudinal velocity gradient at the lower air-water interface ($m^2/s$) |
| $D^{upper}$ | air concentration turbulent diffusivity at the upper air-water interface ($m^2/s$) |
| $d$ | flow depth (m) |
| $d_b$ | particle diameter (m) (water droplet or air bubble) |
| $(d_b)_c$ | maximum particle size (m) in a shear flow |
| $d_0$ | flow depth (m) measured at the edge of the offset |
| $Fr$ | Froude number defined as: $Fr = V/\sqrt{g * d}$ |
| $Fr_0$ | Froude number at the edge of the offset: $Fr_0 = V/\sqrt{g * d_0}$ |
| $g$ | gravity constant ($m/s^2$) |
| $K$ | constant |
| $P_{atm}$ | atmospheric pressure above the flow (Pa) |
| $P_N$ | pressure gradient number defined as: $P_N = \dfrac{\Delta P}{\varrho_w * g * d_0}$ |

| | |
|---|---|
| $Q$ | discharge ($m^3/s$) |
| $Q_{air}^{inlet}$ | air discharge supplied to the aeration device ($m^3/s$) |
| $q$ | discharge per unit width ($m^2/s$) |
| $Tu$ | turbulence intensity: $Tu = u'/V$ |
| $t_r$ | ramp height (m) measured perpendicular to the spillway surface |
| $t_s$ | offset height (m) measured perpendicular to the spillway surface |
| $U_0$ | free stream velocity (m/s) |
| $U_w$ | flow velocity (m/s): $U_w = q_w/d$ |
| $u_r$ | bubble rise velocity (m/s) |
| $u'$ | root mean square of longitudinal component of turbulent velocity (m/s) |
| $V$ | velocity (m/s) |
| $V_{90}$ | velocity (m/s) at which $y = Y_{90}$ |
| $V_{90}^{lower}$ | characteristic velocity (m/s) at which $y = Y_{90}^{lower}$ |
| $V_{90}^{upper}$ | characteristic velocity (m/s) at which $y = Y_{90}^{upper}$ |
| $v'$ | root mean square of lateral component of turbulent velocity (m/s) |
| $v^2$ | spatial average value of the square of the velocity differences over a distance equal to $d_b$ |
| $W$ | channel width (m) |
| $(We)_c$ | critical Weber number |
| $x$ | distance along the spillway bottom (m) |
| $Y_{90}$ | characteristic depth (m) where the air concentration is 90% |
| $Y_{90}^{lower}$ | characteristic depth (m) where the air concentration is 90% at the lower free surface of the jet |
| $Y_{90}^{upper}$ | characteristic depth (m) where the air concentration is 90% at the upper free surface of the jet |
| $y$ | distance from the edge of the deflector measured perpendicular to the spillway surface (m) |
| $y_{50}$ | distance normal to the spillway surface (m) at which $V = U_0/2$ |
| $\alpha$ | spillway slope |
| $\Delta P$ | pressure difference between the atmospheric pressure above the jet and the pressure in the cavity below the jet (Pa) |
| $\nu_T$ | turbulent kinematic viscosity ($m^2/s$) |
| $\theta$ | angle between a streamline and the horizontal |
| $\varrho$ | density ($kg/m^3$) |
| $\sigma$ | surface tension between air and water (N/m) |
| $\Psi^L$ | initial lateral spread angle at the lower jet interface computed between $C = 10\%$ and $C = 90\%$ |
| $\Psi^U$ | initial lateral spread angle at the upper free surface computed between $C = 10\%$ and $C = 90\%$ |

Subscript

| | |
|---|---|
| air | air flow |
| o | flow conditions at the end of the approach flow region |
| w | water flow |

## References / Bibliographie


ACKERS, P. and Priestley, S. J. (1985), Self-Aerated Flow down a Chute Spillway, 2nd Conf. on the Hydraulics of Floods and Flood Control, BHRA, Fluid Engineering, Cambridge, England, pp. 1–16.

CAIN, P. (1978), Measurements within Self-Aerated Flow on a Large Spillway. Ph.D. Thesis, Ref. 78–18, 1978, Univ. of Canterbury, Christchurch, New Zealand.

CAIN, P. and WOOD, I.R. (1981), Measurements of Self-aerated Flow on a Spillway, J. Hyd. Div., ASCE, 107, HY11, pp. 1425–1444.

CHANSON, H. (1988), A Study of Air Entrainment and Aeration Devices on a Spillway Model, Research Rep. 88-8, Oct., Univ. of Canterbury, New Zealand.

CHANSON, H. (1989a), Study of Air Entrainment and Aeration Devices, J. of Hyd. Research, IAHR, Vol. 27, No. 3, pp. 301–319.

CHANSON, H. (1989b), Flow downstream of an Aerator, Aerator Spacing, J. of Hyd. Research, IAHR, Vol. 27, No. 4, pp. 519–536.

CHANSON, H. (1990), Study of Air Demand on Spillway Aerator, J. of Fluids Eng., Trans. ASME, Vol. 112, Sept., pp. 343–350.

CHANSON, H. (1991), Aeration of a Free Jet above a Spillway, J. of Hyd. Research, IAHR, Vol. 29, No. 5, 1991, pp. 655–667.

CHANSON, H. (1992), Air Entrainment in Chutes and Spillways, Research Report No. CE 133, Dept. of Civil Eng., Univ. of Queensland, Australia, Feb., 85 pages.

DODU, J. (1957), Etude de la Couche Limite d'Air autour d'un Jet d'Eau à Grande Vitesse, (Study of the Boundary Layer around a High Velocity Water Jet), Proc. of the 7th IAHR Congress, Lisbon, Portugal, paper D6 (in French).

ERVINE, D. A., MCKEOGH, E. and ELSAWY, E. M. (1980), Effect of Turbulence Intensity on the rate of Air Entrainment by Plunging Water Jets, Proc. Instn Civ. Engrs, Part 2, June, pp. 425–445.

ERVINE, D. A. and FALVEY, H. T. (1987), Behaviour of Turbulent Water Jets in the Atmosphere and in Plunge Pools, Proceedings of the Institution Civil Engineers, Part 2, Mar., 83, pp. 295–314.

GOERTLER, H. (1942), Berechnung von Aufgaben der freien Turbulenz auf Grund eines neuen Näherungsansatzes, Z.A.M.M., 22, pp. 244–254.

HERRINGE, R. A. (1973), A Study of the Structure of Gas-Liquid Mixture Flows, Ph.D. thesis, Univ. of New South Wales, Kensington, Australia.

HINZE, J. O. (1955), Fundamentals of the Hydrodynamic Mechanism of Splitting in Dispersion Processes, J. of AIChE, Vol. 1, No. 3, pp. 289–295.

HOYT, J. W. and TAYLOR, J. J. (1977), Turbulence Structure in a Water Jet Discharging in Air, Physics of Fluids, Vol. 20, No. 10, Pt. II, Oct., pp. S253–S257.

KAWAKAMI, K. (1973), A Study of the Computation of Horizontal Distance of Jet Issued from Ski-Jump Spillway, Proc. of the JSCE, Vol. 219, No. 11, pp. 37–44 (in Japanese).

KILLEN, J. M. (1982), Maximum Stable Bubble Size and Associated Noise Spectra in a Turbulent Boundary Layer, Proc. Cavitation and Polyphase Flow Forum, ASME, pp. 1–3.

LOW, H. S. (1986), Model Studies of Clyde Dam Spillway aerators, Research Report No. 86-6, Dept. of Civil Eng., Univ. of Canterbury, Christchurch, New Zealand.

NASSOS, G. P. and BANKOFF, S. G. (1967), Local Resistivity Probe for Study Point Properties of Gas-Liquid Flows, Can. J. of Chem. Eng., Vol. 45, Oct., pp. 271–274.

RAJARATNAM, N., (1976), Turbulent Jets, Elsevier Scientific Publ. Co., Development in Water Science, 5, New York, USA.

SCHLICHTING, H. (1979), Boundary Layer Theory, McGraw-Hill, New York, USA, 7th edition.

SCHWARTZ, H. I. and NUTT, L. P. (1963), Projected Nappes Subject to Transverse Pressure, J. of Hyd. Div., Proc. ASCE, July, pp. 97–104.

SENE, K. J. (1984), Aspects of Bubbly Two-Phase Flow, Ph.D. thesis, Trinity College, Cambridge, UK, Dec.

SERIZAWA, A., KATAOKA, I. and MICHIYOSHI, I. (1975), Turbulence Structure of Air-Water Bubbly Flows - I. Measuring Techniques, Int. J. Multiphase Flow, Vol. 2, No. 3, pp. 221–233.

SEVIK, M. and PARK, S. H. (1973), The Splitting of Drops and Bubbles by Turbulent Fluid Flow, J. Fluids Engrg., Trans. ASME, March, pp. 53–60.

SHI, Q., PAN, S., SHAO, Y. and YUAN, X. (1983), Experimental Investigation of Flow Aeration to prevent Cavitation Erosion by a Deflector, Shuili Xuebao (J. of Hydraulic Engrg.), Beijing, China, Vol. 3, pp. 1–13 (in Chinese).

TAN, T. P. (1984), Model Studies of Aerators on Spillways, Research Report No. 84-6, Univ. of Canterbury, Christchurch, New Zealand.

THORN, P. F. (1974), Drag Reduction in Fire-Fighting, Proc. of the Intl Conf. on Drag Reduction, BHRA, Sept., paper H1, Cambridge, UK, pp. 1–16.

VAN DE SANDE, E. and SMITH, J. M. (1973), Surface Entrainment of Air by High Velocity Water Jets, Chem. Eng. Science, Vol. 28, pp. 1161–1168.

## APPENDIX 1

### Initial spread angle at the lower air-water interface

Shi et al. (1983), Low (1986) and Chanson (1988) performed air concentration measurements above bottom aeration devices on spillway models. The details of their flow configuration are reported in Table A1. For steep slopes ($\alpha = 49, 51.3, 52.33$ degrees), their results indicate that the spread angle at the lower jet interface $\Psi^L$, computed between $C = 10\%$ and $C = 90\%$, is independent of the pressure gradient across the jet. The results are shown on Fig. 11. For these data, the initial spread angle $\Psi^L$ may be estimated as:

$$\Psi^L = 0.698 * ((U_w)_0)^{0.630} \quad \text{(A1)}$$

with a correlation of 0.643, where $\Psi^L$ is in degrees and $(U_w)_0$ is the mean flow velocity at the edge of the deflector (in m/s). The flow velocity is a measure of the turbulence of the flow, and equation [A1] suggests that the spread angle increases with the level of turbulence.

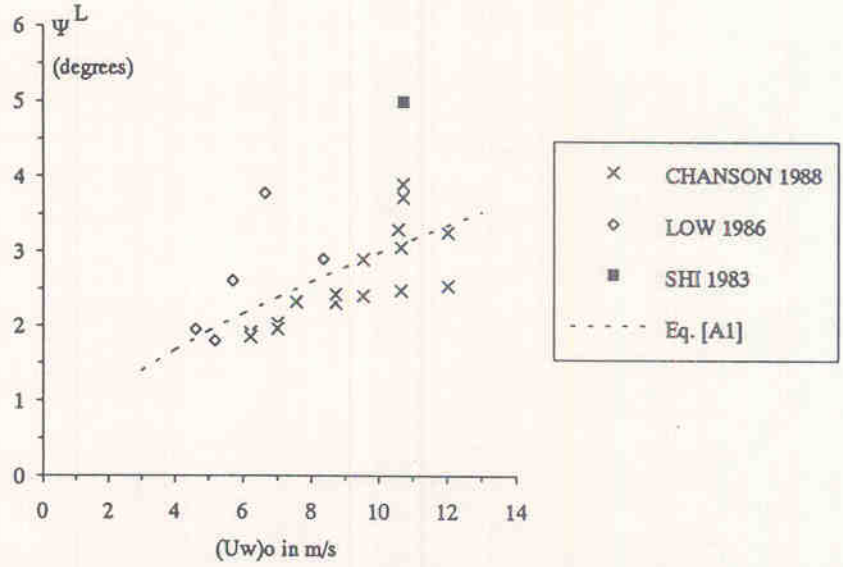


Fig. 11. Initial spread angle at the lower air-water interface - Shi et al. (1983), Low (1986), Chanson (1988).
Angle de dispersion à l'interface inférieure du jet - Shi et al. (1983), Low (1986), Chanson (1988).

Table A1. Flow configurations for air concentration measurements
Configuration des expérimentations de mesures de concentration en air

| ref. (1) | slope $\alpha$ (deg.) (2) | offset height $t_s$ (m) (3) | ramp height $t_r$ (m) (4) | ramp angle (deg.) (5) | Nb exp. (6) | $d_0$ (m) (7) | $Fr_0$ (8) | $P_N$ (9) |
|---|---|---|---|---|---|---|---|---|
| Shi et al (1983) | 49.00 | 0.0 | 0.015 | 5.7 | 1 | 0.058 | 18.6 | 1.0 |
| Low (1986) | 51.30 | 0.03 | 0.03 | 5.7 | 5 | 0.050 | 6-13.5 | 0-0.6 |
| Chanson (1988) | 52.33 | 0.03 | 0.0 | 0.0 | 2 | 0.023 | 19.5 | 0.01-0.5 |
| | | | | | 12 | 0.035 | 10.5-19.5 | 0-1.6 |
| | | | | | 2 | 0.081 | 6.0 | 0.07-0.3 |

Note: Nb exp.: number of experiments
$d_0$: initial fow depth
$Fr_0$: range of Froude numbers
$P_N$: range of pressure gradient numbers